Antiferrodistortive phase transition in $EuTiO_3$

V. Goian,[1] S. Kamba,[1,*] O. Pacherová,[1] J. Drahokoupil,[1] L. Palatinus,[1] M. Dušek,[1] J. Rohlíček,[1] M. Savinov,[1] F. Laufek,[2] W. Schranz,[3] A. Fuith,[3] M. Kachlík,[4,5] K. Maca,[4,5] A. Shkabko,[6] L. Sagarna,[6] A. Weidenkaff,[6] and A. A. Belik[7]

[1]*Institute of Physics ASCR, Na Slovance 2, 182 21 Prague 8, Czech Republic*

[2]*Czech Geological Survey, Geologická 6, 152 00 Prague 5, Czech Republic*

[3]*Faculty of Physics, University of Vienna, Boltzmanngasse 5, A-1090 Wien, Austria*

[4]*Department of Ceramics and Polymers, Brno University of Technology, Technická 2, 616 69 Brno, Czech Republic*

[5]*CEITEC BUT, Brno University of Technology, Technická 10, 616 00 Brno, Czech Republic*

[6]*Swiss Federal Laboratories for Materials Science and Technology, Überlandstrasse 129, 8600 Dübendorf, Switzerland*

[7]*International Center for Materials Nanoarchitectonics (WPI-MANA), National Institute for Materials Science (NIMS), 1-1 Namiki, Tsukuba, Ibaraki 305-0044, Japan*

(Received 28 May 2012; revised manuscript received 20 July 2012; published 17 August 2012)

X-ray diffraction, dynamical mechanical analysis, and infrared reflectivity studies revealed an antiferrodistortive phase transition in $EuTiO_3$ ceramics. Near 300 K, the perovskite structure changes from cubic $Pm\bar{3}m$ to tetragonal $I4/mcm$ due to antiphase tilting of oxygen octahedra along the **c** axis ($a^0a^0c^-$ in Glazer notation). The phase transition is analogous to $SrTiO_3$. However, some ceramics as well as single crystals of $EuTiO_3$ show different infrared reflectivity spectra bringing evidence of a different crystal structure. In such samples, electron diffraction revealed an incommensurate tetragonal structure with modulation wave vector $\mathbf{q} \simeq 0.38\ \mathbf{a}^*$. Extra phonons in samples with modulated structure are activated in the IR spectra due to folding of the Brillouin zone. We propose that defects such as Eu^{3+} and oxygen vacancies strongly influence the temperature of the phase transition to antiferrodistortive phase as well as the tendency to incommensurate modulation in $EuTiO_3$.

DOI: 10.1103/PhysRevB.86.054112 PACS number(s): 61.50.Ks, 78.30.−j, 63.20.−e

I. INTRODUCTION

$EuTiO_3$ is a frequently investigated material in the last decade thanks to Katsufuji and Takagi,[1] who discovered a strong magnetodielectric effect in antiferromagnetic (AFM) G-type phase[2] of this material below $T_N = 5.3$ K. A 7% change of permittivity with magnetic field was found at 2 K. Linear magnetoelectric coupling is forbidden in $EuTiO_3$ due to centrosymmetric structure of this material. Quadratic coupling was not detected, but a strong third-order (bielectrobimagnetic $\sim E^2H^2$) magnetoelectric coupling was observed in Ref. 3. Dielectric permittivity ε' exhibits a typical incipient ferroelectric behavior: ε' increases on cooling and saturates below 50 K.[1] This temperature behavior was explained by an optical phonon softening on cooling and by saturation of its frequency at low temperatures.[4,5] Both temperature dependencies of ε' and soft phonon frequency follow the Barrett formula,[4,5] which takes into account quantum fluctuations at low temperatures. ε' drops down below T_N by several percent due to a strong spin-phonon coupling.[1] In the AFM phase, the temperature and magnetic field dependence of ε' is caused by the response of the lowest-frequency phonon to the magnetic order and/or magnetic field.[6]

Fennie and Rabe[7] suggested to use the spin-phonon coupling and a biaxial strain in the thin $EuTiO_3$ films for induction of ferroelectric and ferromagnetic order, although the bulk $EuTiO_3$ is quantum paraelectric and antiferromagnetic. Recently, Lee *et al.*[8] actually confirmed the theoretical prediction and revealed ferroelectric and ferromagnetic order in the tensile-strained $EuTiO_3$ thin films deposited on $DyScO_3$ substrates. The possibility of inducing the ferroelectric and ferromagnetic order in strained thin films of materials, which are paraelectric and AFM in the bulk form, opens a new route for preparation of novel multiferroics with a strong magnetoelectric coupling and with high critical ordering temperatures. Very promising candidates are $SrMnO_3$,[9] EuO,[10] and $Ca_3Mn_2O_7$.[11]

Until recently, it was assumed that bulk $EuTiO_3$ has perovskite structure with cubic $Pm\bar{3}m$ space group[12] and that the structure is stable down to liquid-He temperatures. However, Rushchanskii *et al.*[13,14] theoretically investigated the structural and lattice dynamical properties of $EuTiO_3$ using first principles and revealed unstable phonons at the R $(\frac{1}{2},\frac{1}{2},\frac{1}{2})$ and M $(\frac{1}{2},\frac{1}{2},0)$ points of the Brillouin zone (BZ) in the cubic structure. Calculated eigenvectors indicated that the instabilities are nonpolar and arise from the tilting and rotation of the oxygen octahedra. The eigenvector for the M-point instable phonon shows in-phase rotations of the oxygen octahedra around one or more pseudocubic axes, whereas at the R point, the octahedra rotate with an alternating out-of-phase sense.[14] Total energy of the possible distorted phases was calculated and three possible stable structures with $R\bar{3}c$, $Imma$, and $I4/mcm$ space groups were suggested. The most stable structure should be $I4/mcm$ ($a^0a^0c^-$ tilts in Glazer notation), second stable structure could be $Imma$ ($a^0b^-b^-$), and the third one the $R\bar{3}c$ structure ($a^-a^-a^-$). However, the energy differences between all the structures are very small (within ~2 meV per formula units), which were within the range of numerical errors. Therefore, all the above-mentioned structures could be realistic and the structural verification is needed. Very recently, specific-heat anomaly measurements revealed an anomaly near 280 K, but the symmetry of the low-temperature structure was not determined.[15] Allieta *et al.*[16] found the structural phase transition at 235 K and determined the low-temperature structure as tetragonal $I4/mcm$. In this paper, we will show that critical temperature (T_c) of the antiferrodistortive phase transition strongly depends on a

quality of the $EuTiO_3$ samples. X-ray diffraction (XRD) and dynamical mechanical analysis of the best $EuTiO_3$ ceramics reveals $T_c = 308$ K, but XRD of single crystal does not resolve the tetragonal symmetry down to 100 K. On the other hand, the electron diffraction reveals tetragonal structure and moreover an incommensurate modulation in single crystal already at room temperature. The reasons for such peculiar effects will be discussed in details.

II. EXPERIMENT

We have investigated single crystals and two kinds of ceramics obtained by different methods. At the beginning, the $EuTiO_3$ powder was prepared from Eu_2O_3 and Ti_2O_3 powders. The initial powder was pelletized and sintered at 1400 °C for 2 h in a pure hydrogen atmosphere. Relative density of such prepared A ceramics was 89% of the theoretical one. Details of the A ceramic preparation are described elsewhere.[17] Ceramics B were prepared from exactly the same $EuTiO_3$ powder as the ceramics A, but the powder was loaded into Au capsules and sintered in a belt-type high-temperature high-pressure furnace at 900 °C under a pressure of 6 GPa for 30 min. Density of the ceramics B was more than 95%.

Single crystals were prepared in two steps. First, a mixture of stoichiometric amounts of Eu_2O_3 (99.9% purity; *Metall Rare Earth Limited*) and TiO_2 (puriss; *Sigma-Aldrich*) was ball-milled and sintered for 10 h at 1000 °*C* under reducing atmosphere (flowing mixture of 5% H_2 in Ar_2, 100 ml/min). The resulting phase was cubic perovskite with $a = 3.905$ Å. Second, the milled powder was pressed into rods with 7-mm diameter and annealed for further 10 h under the same atmosphere. The crystals were grown under flowing mixture of 5% H_2 in Ar (150 ml/min) by using a floating-zone furnace equipped with four halogen lamps (maximum power of 1500 W) and ellipsoidal mirrors. The obtained black crystals after polishing were porosity free with mirror-quality surface. However, the crystals were not perfect; they exhibited mosaicity in the mm-range size. One crystal was grinded for powder x-ray and electron diffraction studies after dielectric, magnetic, and infrared (IR) measurements. For IR studies, the crystal with the size of $3 \times 3 \times 0.15$ mm^3 was generally oriented with [001] axis tilted approximately 30° from the sample normal plane. Therefore, the IR spectra were taken without a polarizer (polarized IR spectra did not show any anisotropy).

The x-ray diffraction studies of ceramics were performed using a Bruker D8 Discover equipped with rotating Cu anode [$\lambda(\mathrm{Cu}K\alpha_1] = 1.540598$ Å; $\lambda(\mathrm{Cu}K\alpha_2) = 1.544426$ Å) working with 12 kW power. A parabolic Göbel mirror was located on the side of the incident beam. Analyzer slits and alternatively also analyzer crystal (200-LiF) were on the side of the diffracted beam. The temperature was controlled by cooling stage Anton Paar DCS 350. The temperature was changed from 173 to 373 K. The x-ray $2\Theta/\Theta$ diffractograms were measured in the broad range of 2Θ angles from 25° till 135° at 193, 293, and 333 K. These whole scans were used for space-group determination and for Rietveld refinement with program TOPAS.[18] Although the analyzer crystal reduces the intensity, it significantly improves the resolution. Thus, it was used for detailed study of the 310 and 420 diffraction peaks (using cubic indexes) that were measured almost each 10 K between 173 and 373 K. Below 300 K, the Rietveld refinements of these two diffraction peaks were performed in $I4/mcm$ space group, because the R_{wp} factor was noticeably lower than in $Pm\bar{3}m$ space group. The fixed microstructure parameters provide precise values of lattice parameters that were used for calculation of the oxygen octahedra tilting angle ϕ (Ref. 19):

$$\cos\phi = \frac{\sqrt{2}a_{\mathrm{tetr}}}{c_{\mathrm{tetr}}}. \quad (1)$$

X-ray diffraction studies of $EuTiO_3$ single crystal were performed with four-circle kappa diffractometer Gemini of Oxford Diffraction (now Agilent Technologies), equipped with CCD detector Atlas. Because of large absorption of the sample, we used Mo$K\alpha$ radiation with doublet $\lambda = 0.7107$ Å, monochromatized with a graphite monochromator and collimated with a fiber-optics Mo-Enhance collimator of Oxford Diffraction. The temperature was controlled with an open-flow cooler Cryojet HT of Oxford Instruments, which uses nitrogen gas as a cooling/heating medium. The measurements were performed at 300 and 100 K.

Electron diffraction patterns were collected at room temperature using transmission electron microscope Philips CM120 equipped with CCD camera Olympus Veleta with 14-bit dynamical range. Crystals of around 500-nm size were investigated. A tilt series of diffraction patterns was recorded ranging from −50° to +50° in steps of 0.5°. This technique is known as electron diffraction tomography.[20] Its main advantages are that it is very fast, does not require the cumbersome procedure of orienting the crystal along some special zone axis, and grant access to a full three-dimensional (3D) intensity distribution in reciprocal space. Oriented reciprocal-space sections were then reconstructed from the raw data by the computer program PETS.[21]

The Young's modulus and thermal expansion were measured using the instrument for dynamical mechanical analysis (DMA 7-Perkin Elmer). The parallel-plate method, described in details elsewhere,[22] was used. The sample dimensions of the parallelepiped were $2.961 \times 0.922 \times 0.745$ mm^3. A static force of 750 mN was modulated by a dynamic force of 700 mN with a frequency of 1 Hz. Nitrogen was used as purge gas.

Low-frequency (1 kHz–1 MHz) dielectric measurements were performed between 2 and 300 K, using NOVOCONTROL Alpha-A High Performance Frequency Analyzer. The magnetic response of the samples was studied with a Vibrating Sample Magnetometer adaptor for the PPMS instrument of Quantum Design. The measurements were performed from room temperature down to 2.5 K under a magnetic field of 100 Oe.

The IR reflectivity spectra were taken using a Bruker IFS 113v FTIR spectrometer at temperatures from 10 to 300 K, with the resolution of 2 cm^{-1}. An Optistat CF cryostat (Oxford Instruments) was used for cooling the samples. The investigated spectral range (up to 650 cm^{-1}) was limited by the transparency region of the polyethylene windows of the cryostat. A helium-cooled Si bolometer operating at 1.6 K was used as a detector. Room-temperature reflectivity was measured up to 3000 cm^{-1}, using pyroelectric deuterated triglicine sulfate detector.

IR reflectivity spectra were carefully fitted assuming the dielectric function in the factorized form of generalized damped harmonic oscillators[23]

$$\varepsilon^*(\omega) = \varepsilon_\infty \prod_{j=1}^{n} \frac{\omega_{\mathrm{LO}j}^2 - \omega^2 + i\omega\gamma_{\mathrm{LO}j}}{\omega_{\mathrm{TO}j}^2 - \omega^2 + i\omega\gamma_{\mathrm{TO}j}}, \tag{2}$$

where $\omega_{\mathrm{TO}j}$ and $\omega_{\mathrm{LO}j}$ denote the transverse and longitudinal frequency of the jth polar phonon, respectively, and $\gamma_{\mathrm{TO}j}$ and $\gamma_{\mathrm{LO}j}$ denote their corresponding damping constants. $\varepsilon^*(\omega)$ is related to the reflectivity $R(\omega)$ of the bulk substrate by

$$R(\omega) = \left| \frac{\sqrt{\varepsilon^*(\omega)} - 1}{\sqrt{\varepsilon^*(\omega)} + 1} \right|^2. \tag{3}$$

The high-frequency permittivity $\varepsilon_\infty = 5.88$ resulting from the electronic absorption processes was obtained from the room-temperature frequency-independent reflectivity tails above the phonon frequencies and was assumed to be temperature independent.

III. RESULTS

A. Structural and elastic properties of the A ceramics

Above room temperature, the x-ray diffraction [see Fig. 1(a)] confirms cubic $Pm\bar{3}m$ structure, which is in complete agreement with Ref. 12. Below 300 K, the structure was refined in $I4/mcm$ space group because the R_{wp} factor was noticeably reduced in this structure. For example, at 273 K, R_{wp} was 9.12 and 12.90 in tetragonal and cubic structures, respectively. Tetragonal $I4/mcm$ structure is obtained by an antiphase tilting of oxygen octahedra along the **c** axis ($a^0a^0c^-$ in Glazer[24] notation). The structure models in $R\bar{3}c$ and $Imma$ space groups were rejected because of discernible discrepancies in the Rietveld refinements. Due to the tetragonal distortion, the lattice parameter splits [see inset of Fig. 1(b)]. The low-temperature value of the splitting is comparable to the theoretical value in Ref. 14. Allieta *et al.* observed the phase transition only at 235 K, but ~130 K below T_c they obtained comparable lattice parameter splitting as we, just their lattice parameters were systematically ~0.003 Å smaller than ours. The temperature dependence of the part of the diffraction pattern close to the 310 reflection is shown in the inset of Fig. 1(a). It is a doublet at high temperatures due to the $K\alpha_1\alpha_2$ lines of Cu, which splits on cooling due to the antiferrodistortive transition. It allowed us to determine the temperature dependence of the tilting angle from the **c** axis [Fig. 1(b)]. One can see that the antiferrodistortive phase transition arises between 295 and 320 K, and the tilt angle ϕ reaches a value of 3.6° at 173 K. The precision of lattice parameters determination was around 0.0001 Å. For very close a and c lattice parameters, it leads to relatively big errors in the determination of ϕ [see Eq. (1)]. For these reasons, the error bars near and above 300 K in Fig. 1(b) are large. At low temperatures, the accuracy of the tilt angle determination is much higher and the error bars are smaller than the dots.

We checked the structure also by electron diffraction on small single-crystalline grains obtained by grinding of A ceramics. The electron diffraction pattern taken at 295 K contains weak spots at the position $h + \frac{1}{2}$, $k + \frac{1}{2}$, $l + \frac{1}{2}$ (see Fig. 2). It confirms tetragonal distortion in ceramics A at room temperature.

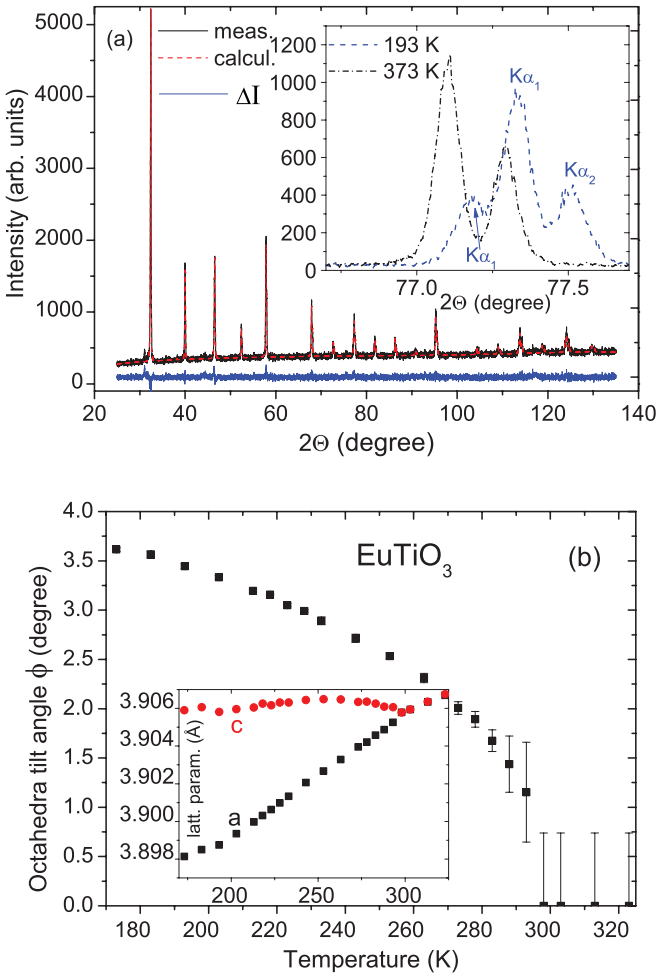

FIG. 1. (Color online) (a) Measured, calculated, and residual x-ray diffraction patterns at 300 K for sample A. The inset shows the splitting of 310 reflection peak on cooling from 373 down to 193 K. Note the $\alpha_1 + \alpha_2$ doublet of 310 reflection. (b) Temperature dependence of tilt angle of oxygen octahedra from the **c** axis. Below 260 K, the error bars are smaller than the points. Inset shows temperature dependence of pseudocubic lattice parameters a and c. Real tetragonal parameters are defined as follows: $a_{\mathrm{tetr}} = \sqrt{2}a$, $c_{\mathrm{tetr}} = 2c$.

The existence of a structural phase transition was confirmed also by other methods. In Fig. 3, we show the temperature dependencies of the thermal expansion and Young's modulus. The curves were systematically measured first on cooling and then on heating. As Fig. 3 shows, the thermal expansion depends linearly on temperature above and below 308 K, indicating that the phase transition at 308 K is of second order. Similar as, e.g., for $SrTiO_3$ (Ref. 25) or $KMnF_3$,[26] the thermal expansion in $EuTiO_3$ is caused by the coupling term which is quadratic in the order parameter and linear in the strain ϵ in a Landau free-energy expansion, implying for the spontaneous strain ϵ_s to be proportional to the square of the order parameter η, i.e., $\epsilon_s \sim \eta^2 \sim (T_c - T)$ for a second-order phase transition. This is also consistent with the observed anomaly in the Young's modulus, which displays a negative dip at T_c followed

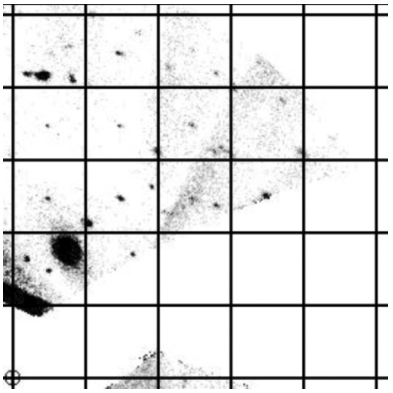

FIG. 2. A reconstructed section of the diffraction pattern of ceramics A showing the layer $\frac{1}{2}kl$. The pseudocubic reciprocal lattice is outlined with grid, point $\frac{1}{2}00$ is marked with a circle in the lower left corner. Additional spots not located at the positions $\frac{1}{2}$, $k+\frac{1}{2}$, $l+\frac{1}{2}$ come from another domain in the crystal.

by a linear increase with decreasing temperature. To describe the elastic anomaly in $EuTiO_3$, we can similarly to $SrTiO_3$ (Ref. 25) employ the leading coupling terms $\sim a\eta^2\epsilon + b\eta^2\epsilon^2$, which leads to

$$E = E^0 - \frac{2a^2}{B} + b\eta^2 \propto E^0 - \frac{2a^2}{B} + (T_c - T) \qquad (4)$$

in perfect agreement with observed behavior (Fig. 3).

Similar dynamical mechanical analysis (DMA) experiments were performed on several $EuTiO_3$ ceramics as well as on ceramics with some pyrochlore or amorphous impurities (all samples prepared by the A method). The phase transition was always observed, but its temperature was reduced in dependence of the impurity concentration. Maximal shift down of the critical temperature was 60 K in samples with ~2% of pyrochlore impurities. Such a low phase transition temperature has been very recently reported by Allieta *et al.*[16] In the high-resolution synchrotron x-ray powder diffraction, they found a signature of the phase transition in $EuTiO_3$ at 235 K. Influence of defects on structural properties of $EuTiO_3$ will be discussed in details in the next section.

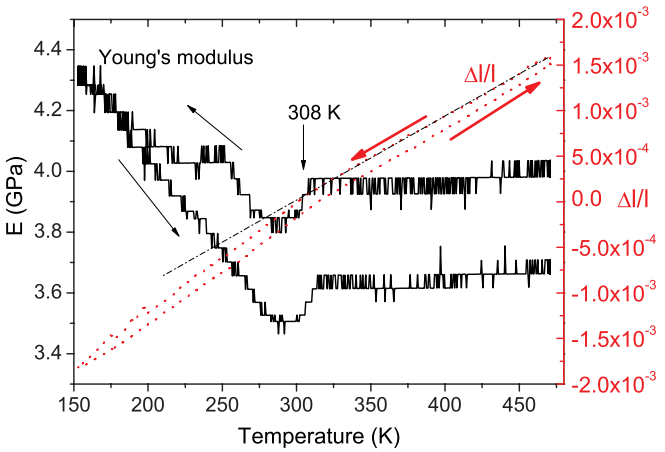

FIG. 3. (Color online) Temperature dependence of Young's modulus E and thermal expansion $\Delta l/l$ in bulk $EuTiO_3$ ceramics sintered by the A method.

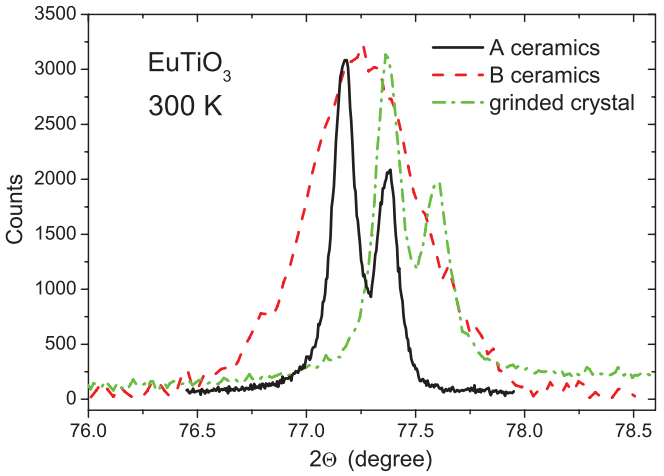

FIG. 4. (Color online) Room-temperature 310 powder diffraction peak of the A and B ceramics compared with the same diffraction peak of grinded single crystal. Higher angle of the diffraction in single crystal gives evidence about its smaller lattice constant than in ceramics. The width of diffraction is broader in the B ceramics due to its smaller crystallite size and larger microstrain. Intensities of all diffractions are normalized for their easier comparison.

B. X-ray diffraction studies of the B ceramics

The B ceramics was sintered at 900 °C and pressure 6 GPa, while the A ceramics was sintered at 1400 °C and ambient pressure. For that reason, smaller crystallite size and larger microstrain (i.e., fluctuation of lattice parameters) is expected in the B ceramics. In Fig. 4 is compared 310 diffraction peak of A and B ceramics together with grinded single crystal. One can see that the diffraction of the B ceramics is very broad and therefore does not allow us to resolve the $K\alpha_1$ and $K\alpha_2$ splitting. From the width of the diffraction, we determined the crystallite size 40 nm and microstrain 0.2%, while in the A ceramics we obtained the crystallite size 90 nm and microstrain 0.03%. Due to large width of diffraction peaks, no structural phase transition could be resolved in the B ceramics down to 100 K. However, we will show in the following that IR spectra give evidence about lower than cubic structure in the B ceramics at all temperatures below 300 K.

C. X-ray and electron diffraction studies of $EuTiO_3$ single crystal

Two small single crystals broken from one larger piece were used for the x-ray diffraction studies. Right-angle triangle with sides 0.2 mm and thickness 0.08 mm showed two grains, while the triangular-shaped sample with sides 0.7 mm and thickness 0.2 mm contained nine single-crystal grains. Within its accuracy and sensitivity, the laboratory single-crystal x-ray diffraction experiment did not reveal any tetragonal distortion or presence of additional spots, as observed in the A ceramics. The cell parameters determined at 100 K were $a =$ 3.89114(11) Å, $b = 3.89144(11)$ Å, $c = 3.89117(10)$ Å, $\alpha =$ 89.984(2)°, $\beta = 90.017(2)°$, $\gamma = 89.984(2)°$ The structure was therefore refined in a cubic space group, yielding R value 0.85% for 74 observed symmetry-independent reflections, with goodness of fit 1.07. Important for successful structure refinement was correction for exceptionally strong extinction.

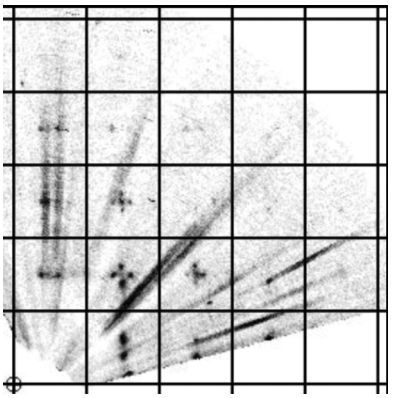

FIG. 5. A reconstructed section of the diffraction pattern of a sample prepared from a monocrystal showing the layer $\frac{1}{2}kl$. The pseudocubic reciprocal lattice is outlined with grid, point $\frac{1}{2}00$ is marked with a circle in the lower left corner. Streaks in the image are traces of thermal diffuse scattering coming from reflections outside the depicted plane.

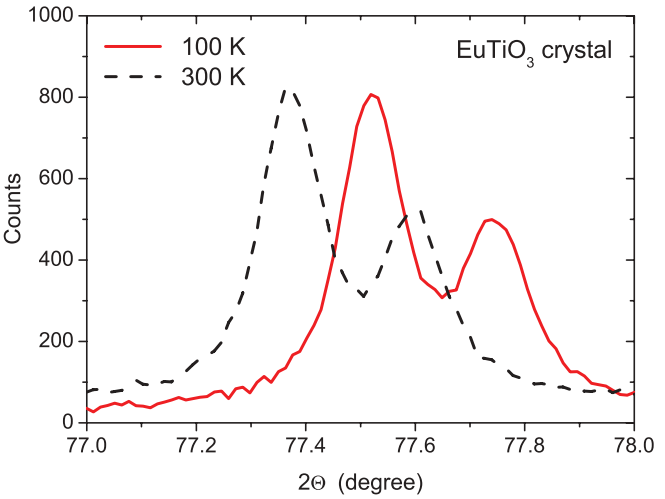

FIG. 6. (Color online) The 310 diffraction peak of grinded single crystal at room temperature and at 100 K. No line broadening or splitting is seen on cooling, i.e., no evidence of tetragonal distortion is revealed.

Many spots, which could be explained by a doubling of the unit cell in the antiferrodistortive phase, were observed, but finally explained by $\lambda/2$ diffraction. After decreasing the voltage on the Mo x-ray tube below the $\lambda/2$ generation limit, i.e., below 34 kV, no such satellite appeared although the loss of intensity due to the decrease of the voltage was fully compensated by increasing the mA rate and the exposition time.

The second larger crystal was grinded 2 h after the x-ray measurements at 100 K and a selected grain of the powder was used for electron diffraction at room temperature. The diffraction pattern (see Fig. 5) reveals weak reflections at positions $h+\frac{1}{2}, k+\frac{1}{2}, l+\frac{1}{2}$, which are evidence for tetragonally distorted phases as in the ceramics A. Moreover, the satellites around these positions are clearly seen in Fig. 5. The satellites show that the structure is incommensurately modulated with modulation wave vector $\mathbf{q}_m = (0.38 \pm 0.02)\,\mathbf{a}^*$.

We repeated the electron diffraction measurements on the same sample two weeks later. No reflections at positions $h+\frac{1}{2}$, $k+\frac{1}{2}$, $l+\frac{1}{2}$ and as well as no incommensurate satellites were observed. The crystal lattice looked cubic. The very recent synchrotron study of Kim *et al.*[27] revealed creation of incommensurate structure in $EuTiO_3$ crystal at 285 K, and the tetragonal distortion appeared only below 160 K. The incommensurate phase transition is of the first order, therefore, it can exhibit some temperature hysteresis. Our first electron diffraction pattern was taken only two hours after cooling to 100 K, therefore we observed the tetragonal distortion and incommensurate modulation at room temperature. After some time, the crystal structure transforms to cubic one at 300 K. We observed temperature hysteresis in tilt angle of oxygen octahedra as well as in T_c with a value of 30–50 K also in the A ceramics.

Our modulation wave vector $\mathbf{q}_m = 0.38\,\mathbf{a}^*$ is smaller than the value $0.43\,\mathbf{a}^*$ reported by Kim *et al.*,[27] but Kim *et al.* have also shown that the incommensurate satellites are strongly time dependent (their position and intensity strongly relaxed within measured 17 h). The time and possible temperature dependencies of the modulation wave vector are probably responsible for the discrepancy between ours and Kim's value of $\mathbf{q}_m$.

Nevertheless, the discrepancy between data obtained using XRD of macroscopic crystal and electron diffraction of the same grinded crystal is remarkable and one could speculate about lower sensitivity of the former method. Therefore, we have decided to use the same grinded crystal for powder x-ray diffraction measurements. The results were rather surprising (see Figs. 4 and 6): (a) The room-temperature lattice constant of the crystal [$a = 3.8966(5)$ Å] is lower than in the A ceramics [$a = 3.9058(5)$ Å]. (b) Diffraction peaks (such as 310 in Fig. 6) do not broaden or split on cooling down to 100 K. It means the lattice of the crystal looks cubic down to 100 K. Note the electron diffraction revealed the incommensurate satellites and tetragonal distortion in grinded single crystal already at room temperature (after cooling to 100 K). Electrons interact much stronger with the crystal than x rays, and the weak intensities can be also enhanced by the dynamical diffraction effects. This could explain the discrepancy between both kinds of experiments. Here, it should be again stressed that the recent x-ray synchrotron investigation of $EuTiO_3$ single crystal, which has the same origin as ours, revealed the tetragonal distortion below 160 K and incommensurate modulation below 285 K.[27]

One can also ask the question, whether the discrepancies between XRD and electron diffraction of the crystals can not be caused by stresses created after grinding of the crystals. It is unlikely that such manipulation would alter the crystal structure. Also, if the material was affected by the crushing, the diffraction pattern would probably show streaking and loss of crystallinity. Moreover, the structure would be most probably different from one grain to another, but we observed the same electron diffraction patterns in three examined crystals. We proved that the material relaxed to its cubic form without satellites in two weeks after the first experiment, indicating strongly a temperature hysteresis.

We tried to see the phase transitions in specific heat of the samples. Unfortunately, we did not detect any anomaly. Our differential scanning calorimeter Perkin Elmer Pyris Diamond

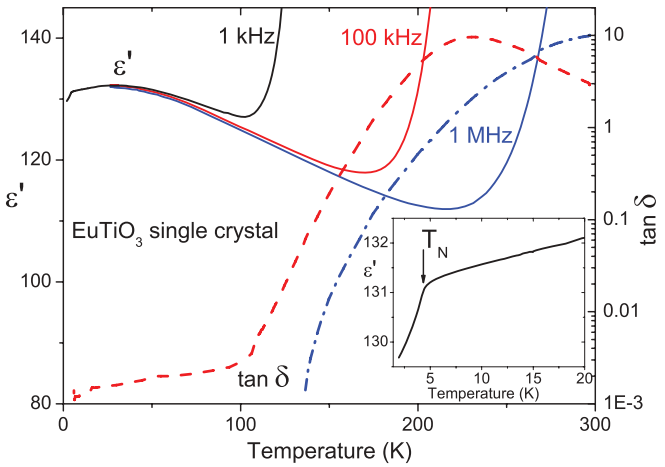

FIG. 7. (Color online) Temperature dependence of dielectric permittivity and loss in $EuTiO_3$ single crystal taken at various frequencies. Inset shows decrease of 1-kHz permittivity below Néel temperature due to spin-phonon coupling.

has probably lower sensitivity than the instrument used in Ref. 15.

Not only structural, but also dielectric and magnetic properties differentiate in various samples. A ceramics has at low temperatures permittivity about 400 (like single crystal in Ref. 1), B ceramics about 200, and the single crystal less than 140 (see Fig. 7). The resistivity was highest in the single crystal, which allowed us to measure intrinsic dielectric permittivity at 1 MHz up to 200 K (Fig. 7), while in the A ceramics permittivity was affected by Maxwell-Wagner polarization already above 80 K.[4] We measured as well magnetic susceptibility and found $T_N = 4.45$ K in single crystal and $T_N = 5.48$ K in the $EuTiO_3$ ceramics and powder, from which the crystal was grown (see Fig. 8). The latter value corresponds to the value reported in the literature.[1,2,4] The reason for lower T_N in single crystal is discussed below.

Our A ceramics exhibits the antiferrodistortive phase transition to tetragonal $I4/mcm$ structure at ~300 K; Köhler *et al.* reported $T_c = 282$ K,[15,28] Allieta *et al.* found $T_c = 235$ K,[16] and Kim *et al.* at 160 K. All the discrepancies in critical temperatures (as well as in the above-mentioned dielectric and magnetic properties) observed in different samples can be explained only by a different concentration of defects (mainly oxygen vacancies and Eu^{3+}). It is known that the oxygen vacancies enhance the lattice constant in isostructural $SrTiO_3$.[29] On the other hand, ionic radius of Eu^{3+} is smaller than ionic radius of Eu^{2+},[30] so the Eu^{3+} defects can reduce the lattice constant in $Eu^{2+}TiO_3$. One can expect that both kinds of defects are mutually connected. Oxygen vacancies can strongly influence the lattice instability to tetragonal phase, where the oxygen octahedral exhibits antiphase tilting. Note as well that Allieta *et al.*[16] observed local fluctuations of the tilt angle, which can be explained by fluctuation of oxygen vacancy concentration. On the other hand, the Eu^{3+} can also reduce the Néel temperature in $EuTiO_3$. It can explain the aforementioned 1 K lower T_N in single crystal than in the ceramics. For that reason, it seems that the $EuTiO_3$ crystal contains more Eu^{3+} defects than the A and B ceramics. Exact determination of concentration of Eu^{3+} and oxygen vacancies using Mössbauer spectroscopy and positron annihilation spectroscopy, respectively, is beyond the scope of this paper, but these experiments are already in progress in our laboratory.

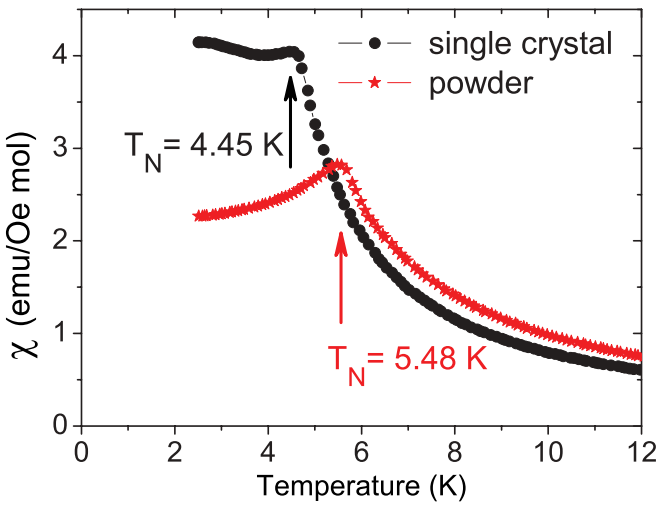

FIG. 8. (Color online) Temperature dependence of magnetic susceptibility in $EuTiO_3$ powder and single crystal.

D. Factor-group analysis

As it was already mentioned above, Rushchanskii *et al.*[14] predicted three possible space groups, in which $EuTiO_3$ could crystallize at low temperatures. Structural analysis can yield sometimes ambiguous results and IR spectra can help in specification of the crystal structure. Before presenting the IR spectra, we perform the factor-group analysis of the optical phonons (i.e., without acoustic modes) in all suggested crystal structures of $EuTiO_3$. In cubic $Pm\bar{3}m$ structure, the analysis gives the following symmetries of phonons in the Γ point of BZ:

$$\Gamma_{Pm\bar{3}m} = 3F_{1u}(x) + F_{2u}(-). \tag{5}$$

The x in brackets means activity in the IR spectra, the $(-)$ marks the silent mode. The factor-group analysis in antiferrodistortive tetragonal $I4/mcm$ phase gives the following:

$$\begin{aligned}\Gamma_{I4/mcm} = {} & 5E_u(x,y) + 3A_{2u}(z) + A_{1g}(x^2+y^2,z^2) \\ & + 3E_g(xz,yz) + 2B_{1g}(x^2-y^2) + 2A_{2g}(-) \\ & + B_{2g}(xy) + A_{1u}(-) + B_{2u}(-).\end{aligned} \tag{6}$$

Here, x^2, xy, etc., mean the components of Raman tensor, where the modes are Raman active. It follows from the analysis that eight polar phonons are expected in IR spectra of tetragonal $EuTiO_3$. Their theoretical frequencies and oscillator strengths are listed in Table I. In the orthorhombic $Imma$ phase, the factor-group analysis yields

$$\begin{aligned}\Gamma_{Imma} = {} & 5B_{1u}(z) + 4B_{2u}(y) + 4B_{3u}(x) + 3A_g(x^2) \\ & + 3B_{2g}(xz) + 4B_{3g}(yz) + 2A_u(-) + 2B_{1g}(xy),\end{aligned} \tag{7}$$

TABLE I. List of phonon ω_{TO} and plasma $\Omega_P = \sqrt{\Delta\varepsilon}\omega_{TO}$ frequencies in $EuTiO_3$ ceramics and single crystal obtained from the fits of IR spectra at 10 K. Experimental parameters are compared with parameters of polar phonons obtained from first-principles calculations (Ref. 14) in different crystal structures. All the parameters are in cm^{-1}.

Mode	A ceramics experiment		$I4/mcm$ theory		B ceramics experiment		$Imma$ theory		Single-crystal experiment		$Pm\bar{3}m$ theory	
assignment	ω_{TO}	Ω_P	ω_{TO}	Ω_P	ω_{TO}	Ω_P	ω_{TO}	Ω_P	ω_{TO}	Ω_P	ω_{TO}	Ω_P
TO1	63	1162	107	1323	82	1290	98	1318	81	742	67	1289
TO1	78	871	128	1607	107	713	110	1233	92	1211		
							131	1596				
TO2	153	329	154	898	154	473	154	822	156	470	155	925
TO2			156	314			155	201				
							159	945				
					220	82	237	134	200	123		
			251	40	277	240	283	122	249	374		
TO3					433	130	416	224	432	61		
TO3	431	348	419	250	442	99	418	230	443	42		
							516	730				
TO4	537	591	523	732	546	672	523	736	541	617	537	824
TO4	570	228	531	718	600	63	537	725	596	103		

while in rhombohedral phase, the optical phonons have the following symmetry in the center of the BZ:

$$\Gamma_{R\bar{3}c} = 5E_u(x,y) + 3A_{2u}(z) + A_{1g}(x^2+y^2,z^2) + 4E_g(xz,yz,x^2-y^2,xy) + 3A_{2g}(-) + 2A_{1u}(-). \quad (8)$$

It means that 13 and 8 IR active phonons are expected in the orthorhombic and rhombohedral phases of $EuTiO_3$, respectively. Let us compare the experimentally observed phonons in various $EuTiO_3$ ceramics and single crystals with the predicted selection rules mentioned above.

E. IR studies

Figure 9 compares the IR reflectivity spectra of the A and B $EuTiO_3$ ceramics with the spectra of a single crystal. Note the similarity between the B ceramics and the single crystal, while the A ceramics has different spectra. The shape of IR spectra of the A ceramics is similar to the previously published spectra.[4,5] At room temperature, three reflection bands marked as TO1, TO2, and TO4 correspond to $3F_{1u}$ symmetry modes of the cubic $Pm\bar{3}m$ structure [see Eq. (5)]. However, at low temperatures, TO1 and TO4 modes split and moreover an additional new mode activates in the spectra near 430 cm^{-1} (see Figs. 9 and 10). Hints of these new modes were observed already in Ref. 4, but that time we interpreted them as impurity modes from the pyrochlore $Eu_2Ti_2O_7$ second phase. However, our spectra obtained from phase pure $EuTiO_3$ A ceramics show the new modes with even higher intensities. Moreover, as we know that the structure of the A ceramics is tetragonal below 300 K, the IR selection rules must be changed [see Eq. (6)]. All TO modes should be split and, moreover, two new E_u symmetry modes should be activated. The new sharp mode seen near 430 cm^{-1} comes from a silent TO3 mode (originally of F_{2u} symmetry in the cubic phase) and it has the E_u symmetry in tetragonal phase [see Eq. (6)]. Another polar mode should be activated around 250 cm^{-1},[14] but its theoretical strength is one order of magnitude lower than that of the other modes (see Table I). For this reason, the mode is not resolved in our spectra.

Phonon eigenfrequencies ω_{TO} and mode plasma frequencies $\Omega_P = \sqrt{\Delta\varepsilon}\omega_{TO}$ of the observed polar phonons in all investigated samples are listed in Table I. These experimental parameters are compared with theoretical values obtained from first principles[14] in tetragonal, orthorhombic, and cubic structures. If we neglect a small theoretical splitting of the TO2 mode, which lies below our spectroscopic resolution, very good agreement of the experimental phonon parameters in the A ceramics and theoretical parameters in the tetragonal $I4/mcm$ structure was obtained.

TO1 phonon splitting was resolved at 250 K, i.e., ~50 K below T_C (see Fig. 10) because the order parameter slowly increases on cooling below T_C. The order parameter exhibits the same temperature dependence as the tilt angle in Fig. 1(b). The new mode has a lower frequency than the original one and softens down to 60 cm (see Fig. 10). This mode was not mentioned in previous publications[4,5] because just a small hint was seen in the IR reflectivity band near 90 cm^{-1}, [Fig. 9(a)]. However, if the TO1 mode is fitted with one oscillator only, its damping increases on cooling,[5] which is not physically meaningful. In our two-component fit of the TO1 band, both phonon dampings decrease on cooling, which is reasonable.

The TO3 mode is seen as a reflectivity minimum near 430 cm^{-1} [see Fig. 9(a)] mainly at low temperature, but the reflectivity fits need this mode at all temperatures up to room temperature. Only the damping of this mode is significantly enhanced at high temperatures, therefore no clear minimum (just sagging) is seen in reflectivity near 430 cm^{-1} close to room temperature. It supports our results in Sec. III A that the A ceramics crystallizes in tetragonal structure already at 300 K.

The B ceramics and single crystal exhibit a very similar IR reflectivity spectra, but different than the A ceramics (see Fig. 9). All together, nine modes were observed in the single-crystal spectra. In comparison to the A ceramics, two

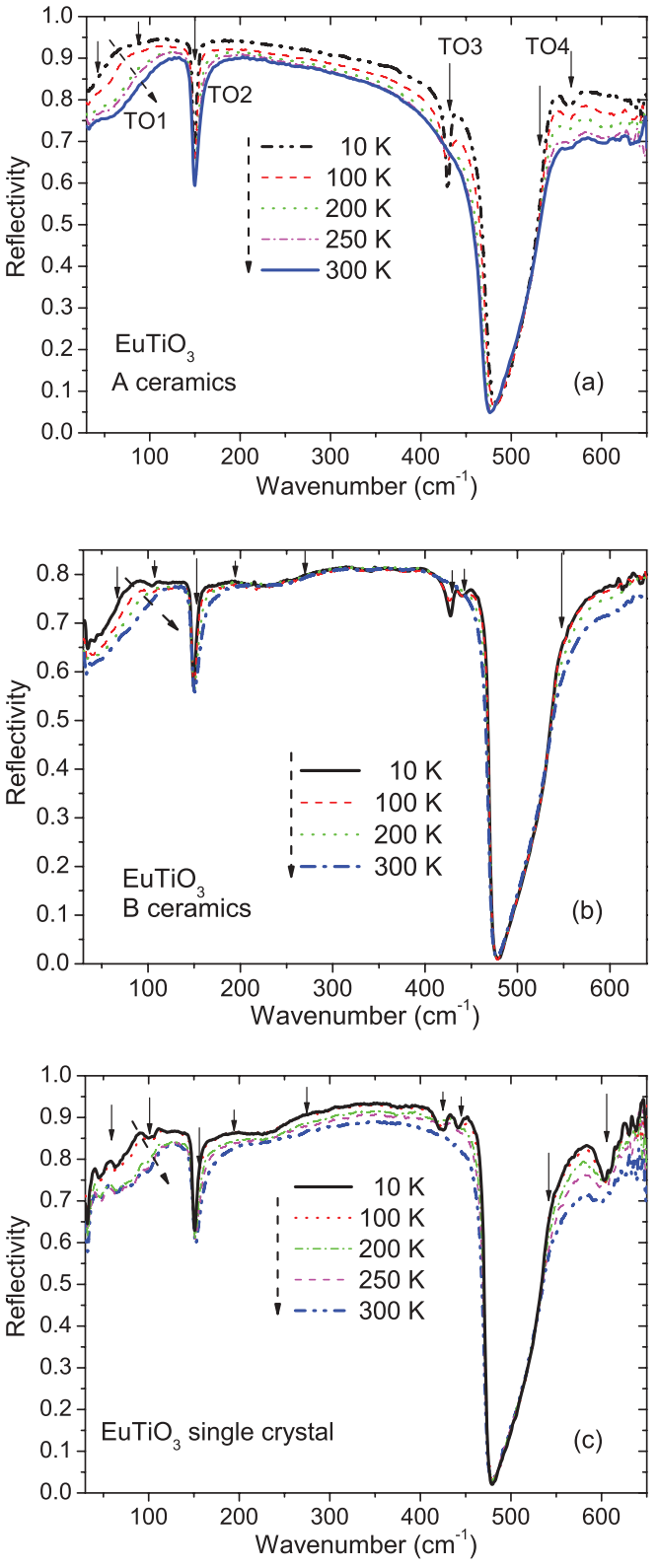

FIG. 9. (Color online) Temperature dependence of IR reflectivity in (a) A ceramics, (b) B ceramics, and (c) single crystal of $EuTiO_3$. Solid arrows mark frequencies of polar phonons. Artificial low-frequency oscillations in the single-crystal spectra are caused by a small size of the crystal.

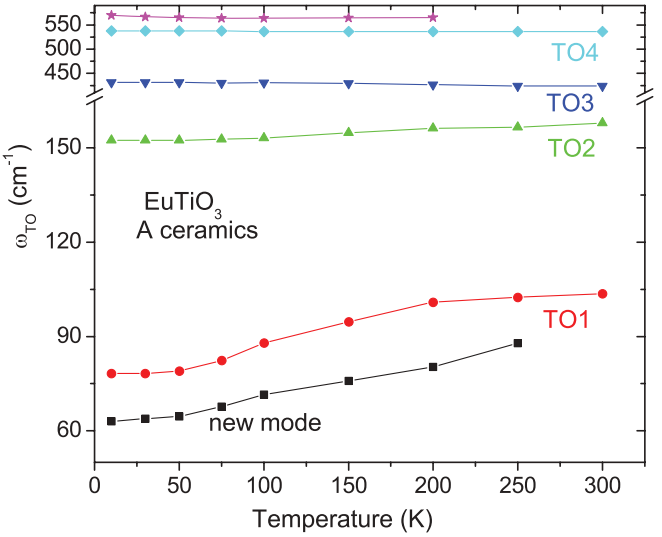

FIG. 10. (Color online) Temperature dependence of the polar phonon frequencies in the A ceramics.

additional phonon bands are seen in single crystal between 200 and 270 cm^{-1} (manifested by bending of reflectivity around 230 cm^{-1}). Moreover, a doublet (instead of a singlet in the A ceramics) arises below 450 cm^{-1} at low temperatures. Their frequencies correspond well to IR active phonons obtained theoretically in the orthorhombic *Imma* structure[14] (see also Table I). Kim *et al.*[27] claim, based on their x-ray synchrotron data, that the structure locally fluctuates between antiferrodistortive and antiferroelectric structure, so one can expect lower than tetragonal symmetry. Our x-ray and electron diffractions do not support the orthorhombic structure, but one should admit that our electron diffraction measurement was not performed below room temperature. Nevertheless, the additional polar phonons seen in the B ceramics and single crystal can be activated due to incommensurately modulated structure. In such a structure, the translation symmetry is broken and the phonon density of states is activated in the IR spectra. In first approximation, newly activated modes are mainly the phonons with the modulation wave vector $\mathbf{q}_m$.[31] One can see that the fingerprint of the modulated structure is the activation of two phonons between 200 and 270 cm^{-1}, which is clearly seen in single crystal and the B ceramics. Also, the splitting of TO3 modes is resolved in both samples at low temperatures. The TO1 and TO4 modes are split in all samples already due to tetragonal distortion. We note that IR spectroscopy is very sensitive on small local breaking of symmetry, which is sometimes hardly resolved in x-ray and electron diffraction experiments.

Rushchanskii *et al.*[14] performed the theoretical analysis of all possible structures in $EuTiO_3$ and came to the conclusion that this material has three different possible ground states with very similar energies. Our structural and IR investigations confirmed a tetragonal structure in the A ceramics prepared by the conventional method. Single crystals exhibit tetragonal distortion and moreover an incommensurate modulation. Small crystallites and large internal microstrain in the B ceramics prepared using high-pressure high-temperature sintering did not allow us to resolve the tetragonal or incommensurate

structure, but according to IR spectra, the structure is the same as in the single crystals. Different structural, infrared, dielectric, and magnetic properties of ceramics and single crystals as well as spread of published phase transition temperatures to tetragonal phase give evidence for a high sensitivity of physical and structural properties of $EuTiO_3$ on concentration of defects in the samples.

IV. CONCLUSION

Until recently, it was assumed that $EuTiO_3$ crystallizes in a stable cubic $Pm\bar{3}m$ structure. Our XRD, electron diffraction, as well as Young's modulus and thermal dilatation studies of conventionally prepared $EuTiO_3$ ceramics (marked as A ceramics) reveal the antiferrodistortive phase transition to tetragonal $I4/mcm$ phase already near 300 K. It is formed by an antiphase tilting of oxygen octahedra along the **c** axis ($a^0a^0c^-$ in Glazer notation). This type of the phase transition, which is the same as in $SrTiO_3$, was very recently confirmed also by other authors, but at different temperatures from 160 to 282 K.[16,27,28] Careful XRD measurements of single crystal as well as grinded crystal did not reveal the tetragonal distortion down to 100 K. On the other hand, electron diffraction of the same grinded crystal, performed at room temperature just after cooling down to 100 K, revealed not only tetragonal but also incommensurate structure, which disappeared after several days. This fact was explained by incommensurate phase transition at 285 K observed very recently by Kim *et al.*[27] because this first-order phase transition can exhibit a temperature hysteresis. We propose to explain the observed discrepancies in structural, infrared, dielectric, and magnetic behavior of ceramics and single crystals as well as various reported critical temperatures by various concentration of Eu^{3+} defects and oxygen vacancies. Their determination using positron annihilation and Mössbauer spectroscopy is currently in progress.

ACKNOWLEDGMENTS

This work was supported by the Czech Science Foundation (Project No. P204/12/1163), MŠMT (COST MP0904 projects LD12026 and LD11035), Project Praemium Academiae of ASCR and the Austrian Science Found (FWF Project No. P23982-N20).

*kamba@fzu.cz

[1] T. Katsufuji and H. Takagi, Phys. Rev. B **64**, 054415 (2001).
[2] T. R. McGuire, M. W. Shafer, R. J. Joenk, H. A. Alperin, and S. J. Pickart, J. Appl. Phys. **37**, 981 (1966).
[3] V. V. Shvartsman, P. Borisov, W. Kleemann, S. Kamba, and T. Katsufuji, Phys. Rev. B **81**, 064426 (2010).
[4] S. Kamba, D. Nuzhnyy, P. Vaněk, M. Savinov, K. Knížek, Z. Shen, E. Šantavá, K. Maca, M. Sadowski, and J. Petzelt, Eur. Phys. Lett. **80**, 27002 (2007).
[5] V. Goian, S. Kamba, J. Hlinka, P. Vaněk, A. A. Belik, T. Kolodizhnyi, and J. Petzelt, J. Eur. Phys. B. **71**, 429 (2009).
[6] S. Kamba, V. Goian, M. Orlita, D. Nuzhnyy, J. H. Lee, D. G. Schlom, K. Z. Rushchanskii, M. Ležaić, T. Birol, C. J. Fennie, P. Gemeiner, B. Dkhil, V. Bovtun, M. Kempa, J. Hlinka, and J. Petzelt, Phys. Rev. B **85**, 094435 (2012).
[7] C. J. Fennie and K. M. Rabe, Phys. Rev. Lett. **97**, 267602 (2006).
[8] J. H. Lee, L. Fang, E. Vlahos, X. Ke, Y. W. Jung, L. Fitting Kourkoutis, J. W. Kim, P. J. Ryan, T. Heeg, M. Roeckerath, V. Goian, M. Bernhagen, R. Uecker, P. C. Hammel, K. M. Rabe, S. Kamba, J. Schubert, J. W. Freeland, D. A. Muller, C. J. Fennie, P. E. Schiffer, V. Gopalan, E. Johnston-Halperin, and D. G. Schlom, Nature (London) **466**, 954 (2010); **476**, 114 (2011).
[9] J. H. Lee and K. M. Rabe, Phys. Rev. Lett. **104**, 207204 (2010).
[10] E. Bousquet, N. A. Spaldin, and P. Ghosez, Phys. Rev. Lett. **104**, 037601 (2010).
[11] N. A. Benedek and C. J. Fennie, Phys. Rev. Lett. **106**, 107204 (2011).
[12] J. Brous, I. Fankuchen, and E. Banks, Acta Crystallogr. **6**, 67 (1953).
[13] K. Z. Rushchanskii, S. Kamba, V. Goian, P. Vaněk, M. Savinov, J. Prokleška, D. Nuzhnyy, K. Knížek, F. Laufek, S. Eckel, S. K. Lamoreaux, A. O. Sushkov, and M. Ležaić, Nat. Mater. **9**, 649 (2010).
[14] K. Z. Rushchanskii, N. A. Spaldin, and M. Ležaić, Phys. Rev. B **85**, 104109 (2012).
[15] A. Bussmann-Holder, J. Köhler, R. K. Kremer, and J. M. Law, Phys. Rev. B **83**, 212102 (2011).
[16] M. Allieta, M. Scavini, L. J. Spalek, V. Scagnoli, H. C. Walker, C. Panagopoulos, S. S. Saxena, T. Katsufuji, and C. Mazzoli, Phys. Rev. B **85**, 184107 (2012).
[17] M. Kachlík, K. Maca, V. Goian, and S. Kamba, Mater. Lett. **74**, 16 (2012).
[18] http://www.bruker-axs.de/topas.html
[19] R. H. Mitchell, *Perovskites: Modern and Ancient* (Almaz, Ontario, Canada, 2002), p.23.
[20] T. E. Gorelik, A. A. Steward, and U. Kolb, J. Microsc. (Oxford, UK) **244**, 325 (2011).
[21] L. Palatinus, PETS (program for analysis of electron diffraction data), Institute of Physics of the AS CR, 2011.
[22] A. V. Kityk, V. P. Soprunyuk, A. Fuith, W. Schranz, and H. Warhanek, Phys. Rev. B **53**, 6337 (1996).
[23] F. Gervais, in *Infrared and Millimeter Waves*, Vol. 8, edited by K. J. Button (Academic, New York, 1983), Chap. 7, p. 279.
[24] M. Glazer, Acta Crystallogr. B **28**, 3384 (1974).
[25] A. V. Kityk, W. Schranz, P. Sondergeld, D. Havlik, E. K. H. Salje, and J. F. Scott, Phys. Rev. B **61**, 946 (2000).
[26] W. Schranz, P. Sondergeld, A. V. Kityk, and E. K. H. Salje, Phys. Rev. B **80**, 094110 (2009).
[27] J.-W. Kim, P. Thomson, S. Brown, P. S. Normile, J. A. Schlueter, A. Shkabko, A. Weidenkaff, and P. J. Ryan, arXiv:1206.5417.
[28] J. Köhler, R. Dinnebier, and A. Bussmann-Holder, arXiv:1205.5374, [Phase Transitions (in press)].
[29] W. Gong, H. Yun, Y. B. Ning, J. E. Greedan, W. R. Datars, and C. V. Stager, J. Solid State Chem. **90**, 320 (1991).
[30] Y. G. Jia, J. Solid State Chem. **95**, 184 (1991).
[31] J. Petzelt, Phase Transitions **2**, 155 (1981).